Padé numerical schemes for the sine-Gordon equation

Francisca Martin-Vergara, Francisco Rus, Francisco R. Villatoro*

[a] *Escuela de Ingenierías Industriales, Dept. de Lenguajes y Ciencias de la Computación, Universidad de Málaga, 29071 Málaga, Spain*

Abstract

The sine-Gordon equation turn up in several problems in science and engineering. Although it is integrable, in practical applications, its numerical solution is powerful and versatile. Four novel implicit finite difference methods based on (q, s) Padé approximations with $(q + s)$-th order in space have been developed and analyzed for this equation; all share the same treatment for the nonlinearity and integration in time. Concretely, $(0, 4)$, $(2, 2)$, $(2, 4)$, and $(4, 4)$ Padé methods; additionally, the energy conserving, Strauss–Vázquez scheme has been considered in a $(0, 2)$ Padé implementation. These methods have been compared among them for both the kink–antikink and breather solutions in terms of global error, computational cost and energy conservation. The $(0, 4)$ and $(2, 4)$ Padé methods are the most cost-effective ones for small and large global error, respectively. Our results indicate that spatial order of accuracy is more relevant to effectiveness of a method than energy conservation even in very long time integrations.

Keywords: Sine-Gordon equation, Padé numerical methods, Implicit time integration, Solitons

1. Introduction

The sine-Gordon equation (sGE) arises in many branches of mathematical physics. It was discovered in the study of surfaces of constant negative curvature. It is also a continuum model for waves in coupled-pendulum, mechanical systems, the magnetic-flux propagation in large Josephson junctions, the study of the domain wall dynamics in magnetic crystals, the propagation of crystal dislocations in solids, the propagation of ultra-short optical pulses in optical fibers, and as a nonlinear, effective, field theory for strong interactions in particle physics, among others [1, 2, 3]. The sGE is exactly solvable by the inverse scattering method [4, 5, 6, 7], however it still continues to provide mathematical surprises and new physical applications [3], such in graphene superlattices [8].

*Corresponding author: Tel.: +34-951952388; fax: +34-951952542.
Email addresses: fmarver@uma.es (Francisca Martin-Vergara), fdrus@uma.es (Francisco Rus), frvillatoro@uma.es (Francisco R. Villatoro)

Let us briefly review the current state of the numerical solution of the sGE. The first two numerical methods for the sGE were developed by Perring and Skyrme (PS), a method of characteristics and a leapfrog finite difference scheme [9]. A staggered-leapfrog scheme was introduced by Ablowitz, Kruskal, and Ladik (AKL) with the goal of stabilizing the PS scheme [10]. An energy-conserving, implicit, leapfrog finite difference scheme was developed by Strauss and Vázquez (SV) for the Klein–Gordon equation [11], first used for the sGE in Ref. [12]. A comparison of four leapfrog numerical schemes, the PS, AKL, SV, and a new fully-explicit method shows that, for long-time integration, the SV scheme is the best one [13]. Several generalizations of the SV scheme, also energy-conserving and second-order in both space and time, have been published [14, 15, 16, 17, 18]; the comparison among these methods shows that implicitness is the key property for long-time stability, instead of energy conservation [19]. However, a general procedure for the development of energy-conserving methods based on the nonlinear treatment of the SV scheme [20] and starting from a discrete energy [21] have been developed.

Finite difference schemes based on (q, s) Padé approximants, with $(q + s)$-th order in space, are also referred to as compact operator methods. Bratsos and Twizell [22] used $(0, 2)$, $(1, 1)$, and $(1, 2)$ Padé methods, Duncan [23] and Bratsos [24] a $(2, 2)$ one, and Sari and Güarslan [25] a $(2, 4)$ one, all with the nonlinearity treatment of the PS scheme; a comparison of some of the Padé methods with PS, AKL, and SV schemes shows that high-order methods are more efficient for high accuracy [23]. Other Padé methods up to fourth-order have been developed in Refs. [26, 27, 28], however, up to these authors' knowledge, Padé methods with the nonlinearity treatment of the SV scheme have not been either developed or analyzed.

Apart from finite differences, other numerical methods have also been used for the sGE. Pseudospectral methods, like the split-step Fourier scheme [29, 30, 31], and spectral methods like an energy-conserving, Fourier scheme [32], a Legendre spectral element method [33], a wavelet spectral method [34, 35], and a multiresolution analysis method based on Legendre wavelets [36]. Finite element methods based on a Petrov–Galerkin scheme [37], and on a collocation scheme using Legendre–Gauss–Lobatto points [38], or cubic B-splines [39]. Multisymplectic methods [40, 41], including a systematic method for discretizing Hamiltonian partial differential equations preserving their energy exactly [32, 42], even for arbitrary boundary conditions [43]. Moreover, meshless methods based on multiquadric quasi-interpolation [44, 45], on radial basis fuctions [46, 47], and on an optimal nodal distribution determined by the so-called optimal sampling density of kernel interpolation time variables [48]. Even, exponentially-fitted and piecewise analytical methods [49], boundary element methods [50], local discontinuous Galerkin methods [51, 52], and numerical implementations of the inverse scattering transform have been developed for the sGE [53, 54]. Finally, note that many of these methods have been extended to two and three dimensions [55].

Previous studies [23, 31, 35] pointed out that the spatial order of accuracy is more important for accuracy than either the symplectic or the energy conser-

vation property; although some authors have results that do not seem to agree with it [49]. Hence, high-order methods must be explored. The goal of this paper is to develop Padé methods with the nonlinearity treatment of the SV scheme.

The contents of this paper are as follows. Section 2 presents the five numerical Padé approximation schemes for the sGE; their linear stability is studied in Subsection 2.1. A detailed comparison of these methods is presented in Section 3, for the propagation of both a kink-antikink solution in Subsection 3.1, and a breather in Subsection 3.2. Finally, the last section is devoted to some conclusions.

2. Numerical schemes

The initial-value problem for the sine-Gordon equation is written in non-dimensional form as

$$\frac{\partial^2 u}{\partial t^2} - \frac{\partial^2 u}{\partial x^2} + \frac{dF(u)}{du} = 0, \qquad x \in \mathbb{R}, \quad t \geq 0, \tag{1}$$

$$u(x,0) = u_0(x), \qquad \frac{\partial u}{\partial t}(x,0) = u_1(x), \tag{2}$$

where $F(u) = 1 - \cos(u)$ is the potential energy, with $F_u(u) \equiv dF(u)/du = \sin(u)$, and $u(x,t)$ denotes the amplitude of the solution, x is the spatial coordinate, and t is time. The existence, uniqueness, and regularity of the solutions of the initial-boundary value problem for the sGE can be proved by using the same approach as for the inhomogeneous, linear wave equation; it is sufficient to show the contractivity of Duhamel's formula as a nonlinear integral operator. In fact, Theorem B.5 in Ref. [56, Appendix B] states that for $u_0(x) \in L^p(\mathbb{R})$, $\partial u_0(x)/\partial x \in L^p(\mathbb{R})$, and $u_1(x) \in L^p(\mathbb{R})$, the unique weak solution of the sGE for $t \in [0,T]$ is $u(x,t) \in L^p(\mathbb{R}) \times L^\infty[0,T]$. Hence, high-order numerical methods can be applied without concern for consistency, since for enough regularity in the initial condition, the classical solution achieves the same regularity.

The sGE is integrable in the sense of Liouville, having an infinite set of conservation laws. In order to assess the accuracy of the numerical methods, let us use the momentum and the energy, given by

$$P(t) = -\int_{-\infty}^{\infty} \left(\frac{\partial u}{\partial t}\right) \left(\frac{\partial u}{\partial x}\right) dx = P(0), \tag{3}$$

$$E(t) = \int_{-\infty}^{\infty} \left(\frac{1}{2} \left(\frac{\partial u}{\partial t}\right)^2 + \frac{1}{2} \left(\frac{\partial u}{\partial x}\right)^2 + F(u) \right) dx = E(0), \tag{4}$$

respectively. Since $F(u)$ is positive definite, it can be shown that $|P(t)| \leq E$; moreover, the speed of the kinks (antikinks) can be calculated as $v(t) = P(t)/E(t)$, thanks to the negative sign in the definition of the momentum.

Let us consider five numerical methods for the solution of Eq. (1) by using Padé approximants in space, all with the same central, second-order differences in time, and an approximation of the nonlinear term inspired in the conservative method of Strauss–Vázquez [11]. The resulting scheme can be written as

$$\mathcal{A}_i(\mathrm{E})\,\frac{U_m^{n+1}-2\,U_m^n+U_m^{n-1}}{\Delta t^2}-\mathcal{B}_i(\mathrm{E})\,U_m^n+\mathcal{A}_i(\mathrm{E})\,H(U_m^{n+1})=0, \tag{5}$$

with

$$H(U_m^{n+1})\equiv\frac{F(U_m^{n+1})-F(U_m^{n-1})}{U_m^{n+1}-U_m^{n-1}}, \tag{6}$$

where $U_m^n\approx u(x_m,t^n)=u_m^n$, with $x_m=m\,\Delta x$, $m\in\mathbb{Z}$, with Δx as the grid size, and $t^n=n\,\Delta t$, $n\in\mathbb{N}$, with Δt as the time step, and $\mathcal{A}_i^{-1}(\mathrm{E})\,\mathcal{B}_i(\mathrm{E})\,u_m^n$ is the i-th Padé approximation for the second-order spatial derivative of $u(x_m,t^n)$ in Method i, with E being the shift operator, i.e., $\mathrm{E}\,U_m^n=U_{m+1}^n$. Hereon, for the numerical solution of the initial-value problem of Eq. (1), periodic boundary conditions are used in the finite interval $x\in(-L/2,L/2]$, with $x_m=-L/2+m\,\Delta x$, $m=1,2,\ldots,M$, and $\Delta x=L/M$ (note that $x_0\equiv x_M$), and a finite time interval $t\in[0,T]$, with $t^n=n\,\Delta t$, $n=0,1,\ldots,N$, and $\Delta t=T/N$.

Method (5) is implicit, since the calculation of U_m^{n+1} from U_m^n and U_m^{n-1} requires the solution of a nonlinear equation. Let us use Newton's iterative method given by

$$\begin{aligned}&\mathcal{A}_i(\mathrm{E})\,\left(U_m^{(k+1)}-2\,U_m^n+U_m^{n-1}\right)-\Delta t^2\,\mathcal{B}_i(\mathrm{E})\,U_m^n\\&\quad+\Delta t^2\,\mathcal{A}_i(\mathrm{E})\,\left(H(U_m^{(k)})+H_u(U_m^{(k)})\,(U_m^{(k+1)}-U_m^{(k)})\right)=0,\end{aligned} \tag{7}$$

with

$$H_u(U_m^{(k)})\equiv\frac{F_u(U_m^{(k)})\,(U_m^{(k)}-U_m^{n-1})-(F(U_m^{(k)})-F(U_m^{n-1}))}{\left(U_m^{(k)}-U_m^{n-1}\right)^2}. \tag{8}$$

Our stopping criterion for Newton's iteration convergence is based on the relative error using the infinite norm, i.e., $\|U_m^{(k+1)}-U_m^{(k)}\|_\infty\le\mathrm{Tol}\,\|U_m^{(k+1)}\|_\infty$, with $\|U_m^{(k)}\|_\infty=\max_m|U_m^{(k)}|$, and Tol being a small enough tolerance.

There are catastrophic cancellations in the numerical evaluation of Eq. (6) for $H(U)$, and Eq. (8) for $H_u(U)$, when $|U-U_m^{n-1}|\ll 1$. For the sGE, they can be avoided by rearranging the expression of $H(U)$ by means of the exact formula [17, 32, 42]

$$H(U)=\frac{\cos(U)-\cos(U_m^{n-1})}{U-U_m^{n-1}}=\frac{2\,\sin((U+U_m^{n-1})/2)\,\sin((U-U_m^{n-1})/2)}{U-U_m^{n-1}},$$

and that of $H_u(U)$ by means of

$$H_u(U)=\frac{\sin(U)}{U-U_m^{n-1}}-\frac{2\,\sin((U+U_m^{n-1})/2)\,\sin((U-U_m^{n-1})/2)}{\left(U-U_m^{n-1}\right)^2}.$$

The local truncation error terms $\mathcal{L}_i(u)$ of Method i can be easily calculated as follows; note that for smooth initial conditions the solution is smooth in both space and time. By using Taylor series expansion after the substitution of U_m^n by the exact solution $u(x_m, t^n)$ in Eq. (5) for the i-th method results in

$$\mathcal{M}_i(u) \equiv \mathcal{G}(u) + \mathcal{L}_i(u) = 0, \tag{9}$$

where $\mathcal{G}(u)$ is the sGE, cf.

$$\mathcal{G}(u) \equiv \frac{\partial^2 u}{\partial t^2} - \frac{\partial^2 u}{\partial x^2} + \sin(u),$$

and the local truncation error is

$$\mathcal{L}_i(u) = \mathcal{T}(u)\,\Delta t^2 + \mathcal{S}_i(u)\,\Delta x^{p_i} + \text{h.o.t.}, \tag{10}$$

where h.o.t. stands for higher-order terms depending on u and its partial derivatives, p_i is the approximation order of the Padé operator for i-th method, and

$$\mathcal{T}(u) = -\frac{1}{6}\,\sin(u)\,\left(\frac{\partial u}{\partial t}\right)^2 + \frac{1}{2}\,\cos(u)\,\frac{\partial^2 u}{\partial t^2} + \frac{1}{12}\,\frac{\partial^4 u}{\partial t^4}.$$

Method 1. The finite difference method developed by Strauss and Vázquez [11] is interpreted as a (0,2)-Padé method by using

$$\mathcal{A}_1(\mathrm{E}) = \mathcal{I},$$

$$\mathcal{B}_1(\mathrm{E}) = \frac{\mathrm{E}^{-1} - 2 + \mathrm{E}^1}{\Delta x^2},$$

where $\mathcal{I}$ is the identity operator. Method 1 is second-order accurate in space ($p_1 = 2$) since

$$\frac{\mathcal{B}_1(\mathrm{E})}{\mathcal{A}_1(\mathrm{E})}\,u(x_m, t^n) = \frac{\partial^2 u}{\partial x^2} + \frac{\Delta x^2}{12}\,\frac{\partial^4 u}{\partial x^4} + \mathcal{O}(\Delta x^4).$$

The local truncation error for the Strauss–Vázquez method, $\mathcal{L}_1(u)$ in Eq. (10), is given by

$$\mathcal{L}_1(u) = \mathcal{T}(u)\,\Delta t^2 - \frac{\Delta x^2}{12}\,\frac{\partial^4 u}{\partial x^4} + \text{h.o.t.}\,. \tag{11}$$

Method 2. A novel (0,4)-Padé method of fourth-order in space, inspired in the method of lines developed by Duncan [23, section 2.5] using symplectic and Dormand–Prince, Runge–Kutta methods, but with the SV scheme for the nonlinearity, given as

$$\mathcal{A}_2(\mathrm{E}) = \mathcal{I},$$

$$\mathcal{B}_2(\mathrm{E}) = \frac{-\mathrm{E}^{-2} + 16\,\mathrm{E}^{-1} - 30 + 16\,\mathrm{E}^1 - \mathrm{E}^2}{12\,\Delta x^2}.$$

By using Taylor series expansion, the Padé operator yields

$$\frac{\mathcal{B}_2(\mathrm{E})}{\mathcal{A}_2(\mathrm{E})}\,u(x_m,t^n) = \frac{\partial^2 u}{\partial x^2} - \frac{\Delta x^4}{90}\,\frac{\partial^6 u}{\partial x^6} + \mathcal{O}(\Delta x^6).$$

The local truncation error for this method is given by

$$\mathcal{L}_2(u) = \mathcal{T}(u)\,\Delta t^2 + \frac{\Delta x^4}{90}\,\frac{\partial^6 u}{\partial x^6} + \text{h.o.t.}. \tag{12}$$

Method 3. A novel (2,2)-Padé method of fourth-order in space, inspired in the compact operator methods used by Duncan [23, section 2.4], but incorporating the SV scheme for the nonlinearity, which can written as

$$\mathcal{A}_3(\mathrm{E}) = \frac{\mathrm{E}^{-1} + 10 + \mathrm{E}^{1}}{12},$$

$$\mathcal{B}_3(\mathrm{E}) = \frac{\mathrm{E}^{-1} - 2 + \mathrm{E}^{1}}{\Delta x^2},$$

which approximates the second-order derivative up to the fourth-order, as shown by Taylor series expansion,

$$\frac{\mathcal{B}_3(\mathrm{E})}{\mathcal{A}_3(\mathrm{E})}\,u(x_m,t^n) = \frac{\partial^2 u}{\partial x^2} - \frac{\Delta x^4}{240}\,\frac{\partial^6 u}{\partial x^6} + \mathcal{O}(\Delta x^6).$$

The local truncation error for this method is given by

$$\mathcal{L}_3(u) = \mathcal{T}(u)\,\Delta t^2 + \frac{\Delta x^4}{240}\,\frac{\partial^6 u}{\partial x^6} + \text{h.o.t.}. \tag{13}$$

Method 4. A novel (2,4)-Padé method of sixth-order in space, with the SV scheme for the nonlinearity, given by

$$\mathcal{A}_4(\mathrm{E}) = \frac{2\,\mathrm{E}^{-1} + 11 + 2\,\mathrm{E}^{1}}{3},$$

$$\mathcal{B}_4(\mathrm{E}) = \frac{\mathrm{E}^{-2} + 16\,\mathrm{E}^{-1} - 34 + 16\,\mathrm{E}^{1} + \mathrm{E}^{2}}{4\,\Delta x^2},$$

which can be easily checked by Taylor series expansion yielding

$$\frac{\mathcal{B}_4(\mathrm{E})}{\mathcal{A}_4(\mathrm{E})}\,u(x_m,t^n) = \frac{\partial^2 u}{\partial x^2} + \frac{23\,\Delta x^6}{75600}\,\frac{\partial^8 u}{\partial x^8} + \mathcal{O}(\Delta x^8).$$

In this case, the local error is

$$\mathcal{L}_4(u) = \mathcal{T}(u)\,\Delta t^2 - \frac{23\,\Delta x^6}{75600}\,\frac{\partial^8 u}{\partial x^8} + \text{h.o.t.}. \tag{14}$$

Method 5. A novel (4,4)-Padé method of eighth-order in space, with the SV scheme for the nonlinearity, which can be written as

$$\mathcal{A}_5(\mathrm{E}) = \frac{23\,\mathrm{E}^{-2} + 688\,\mathrm{E}^{-1} + 2358 + 688\,\mathrm{E}^{1} + 23\,\mathrm{E}^{2}}{15},$$

$$\mathcal{B}_5(\mathrm{E}) = \frac{31\,\mathrm{E}^{-2} + 128\,\mathrm{E}^{-1} - 318 + 128\,\mathrm{E}^{1} + 31\,\mathrm{E}^{-2}}{\Delta x^2},$$

whose accuracy can be verified by Taylor series expansion resulting in

$$\frac{\mathcal{B}_5(\mathrm{E})}{\mathcal{A}_5(\mathrm{E})}\,u(x_m,t^n) = \frac{\partial^2 u}{\partial x^2} - \frac{79\,\Delta x^8}{4762800}\,\frac{\partial^{10} u}{\partial x^{10}} + \mathcal{O}(\Delta x^{10}).$$

In this case, the local error is

$$\mathcal{L}_5(u) = \mathcal{T}(u)\,\Delta t^2 + \frac{79\,\Delta x^8}{4762800}\,\frac{\partial^{10} u}{\partial x^{10}} + \text{h.o.t.}\,. \tag{15}$$

For a fair comparison of the five methods the discrete analogue of the energy (4) given by

$$E^n = \Delta x \sum_m \left[\frac{1}{2}\left(\frac{U_m^{n+1} - U_m^n}{\Delta t}\right)^2 + \frac{1}{2}\left(\frac{U_{m+1}^{n+1} - U_m^{n+1}}{\Delta x}\right)\left(\frac{U_{m+1}^{n} - U_m^{n}}{\Delta x}\right)\right] + \Delta x \sum_m \left[\frac{F(U_m^{n+1}) + F(U_m^{n-1})}{2}\right], \tag{16}$$

is used; this discrete energy is exactly conserved ($E^n = E^0$) by the SV method [11]. Neither of the Methods 2–5 exactly conserve it.

In order to numerically estimate the speed of the kinks (antikinks) by means of $v(t) = P(t)/E(t)$, a discrete analogue of the momentum (3) given by

$$P^n = -\Delta x \sum_m \left[\left(\frac{U_m^{n+1} - U_m^{n-1}}{2\,\Delta t}\right)\left(\frac{U_{m+1}^{n} - U_{m-1}^{n}}{2\,\Delta x}\right)\right], \tag{17}$$

has been used [11]. Note that neither of the Methods 1–5 exactly conserve this discrete momentum.

2.1. Stability analysis

The linear stability of Methods 1–5 can be easily studied by means of using the von Neumann analysis. The computational error $Z_m^n = U_m^n - U_m^{n*}$, with respect to a given solution U_m^{n*}, can be Fourier expanded as $Z_m^n = \exp(\mathrm{i}\,m\,\beta\,\Delta x)\,\xi^n$, where $\mathrm{i} = \sqrt{-1}$, β is the spatial frequency, and ξ is the amplification factor, and substituted into Eq. (5) with $F \equiv 0$. After cancelling common factors, the resulting polynomial equation for ξ is given by

$$p_i(\xi) = A_i\,\xi^2 - 2\,B_i\,\xi + A_i = 0, \tag{18}$$

whose two roots ξ_1 and ξ_2 have modulus smaller than or equal to unity for every ξ if and only if $|B_i| \leq A_i$, i.e., $-A_i \leq B_i \leq A_i$. These two inequalities yield necessary condition for linear stability on both Δx and Δt.

Method 1. The (linear) stability polynomial (18) for the Strauss–Vázquez method has coefficients

$$A_1 = 1, \qquad B_1 = 1 - 2\,r^2\,\sin^2(\omega), \tag{19}$$

where $r = \Delta t/\Delta x$, and $\omega = \beta\,\Delta x/2$. For stability, the condition $B_1 \leq A_1$ is always true, and the condition $-A_1 \leq B_1$ gives

$$2\,r^2\,\sin^2(\omega) \leq 2,$$

$$\left(\frac{\Delta t}{\Delta x}\right)^2 \leq 1, \qquad \Delta t \leq \Delta x. \tag{20}$$

Note that this is the CFL condition.

Method 2. The stability polynomial (18) for this method is given by

$$A_2 = 1, \qquad B_2 = 1 - \frac{8\,r^2}{3}\,\sin^2(\omega) + \frac{r^2}{6}\,\sin^2(2\,\omega). \tag{21}$$

In this case, the condition $B_2 \leq A_2$ yields

$$0 \leq \frac{8}{3}\,\sin^2(\omega) - \frac{1}{6}\,\sin^2(2\,\omega) \leq \frac{8}{3},$$

being always true, and the condition $-A_2 \leq B_2$ gives

$$r^2\,\left(\frac{8}{3}\,\sin^2(\omega) - \frac{1}{6}\,\sin^2(2\,\omega)\right) \leq 2,$$

$$\left(\frac{\Delta t}{\Delta x}\right)^2 \leq \frac{3}{4}, \qquad \Delta t \leq \frac{\sqrt{3}}{2}\,\Delta x \leq \Delta x. \tag{22}$$

Method 3. This method has a stability polynomial (18) with coefficients

$$A_3 = 1 - \frac{1}{3}\,\sin^2(\omega), \tag{23}$$

$$B_3 = 1 - \frac{1}{3}\,\sin^2(\omega) - 2\,r^2\,\sin^2(\omega). \tag{24}$$

In this case, the condition $B_3 \leq A_3$ is always true, and the condition $-A_3 \leq B_3$ gives

$$2\,r^2\,\sin^2(\omega) \leq 2 - \frac{2}{3}\,\sin^2(\omega),$$

$$2\,r^2\,\sin^2(\omega) \le 2 - \frac{2}{3} = \frac{4}{3},$$

$$\left(\frac{\Delta t}{\Delta x}\right)^2 \le \frac{2}{3}, \qquad \Delta t \le \frac{\sqrt{6}}{3}\,\Delta x \le \Delta x. \tag{25}$$

Method 4. The stability polynomial (18) of this method is given by

$$A_4 = 5 - \frac{8}{3}\,\sin^2(\omega), \tag{26}$$

$$B_4 = 5 - \frac{8}{3}\,\sin^2(\omega) - 8\,r^2\,\sin^2(\omega) - \frac{r^2}{2}\,\sin^2(2\,\omega). \tag{27}$$

In this case, the condition $B_4 \le A_4$ is always true, and the condition $-A_4 \le B_4$ gives

$$r^2\,\left(8\,\sin^2(\omega) + \frac{1}{2}\,\sin^2(2\,\omega)\right) \le 10 - \frac{16}{3}\,\sin^2(\omega),$$

$$\left(\frac{\Delta t}{\Delta x}\right)^2 \le \frac{7}{12}, \qquad \Delta t \le \frac{\sqrt{21}}{6}\,\Delta x \le \Delta x. \tag{28}$$

Method 5. The stability polynomial (18) of this method is given by

$$A_5 = 252 - \frac{2752}{15}\,\sin^2(\omega) - \frac{92}{15}\,\sin^2(2\,\omega), \tag{29}$$

$$B_5 = 252 - \frac{2752}{15}\,\sin^2(\omega) - \frac{92}{15}\,\sin^2(2\,\omega) \tag{30}$$

$$- 504\,r^2\,\sin^2(\omega) + 248\,r^2\,\sin^4(\omega). \tag{31}$$

In this case, the condition $B_5 \le A_5$ is always true, and the condition $-A_5 \le B_5$ gives

$$r^2\,\left(504\,\sin^2(\omega) - 248\,\sin^4(\omega)\right) \le \left(504 - \frac{5504}{15}\,\sin^2(\omega) - \frac{184}{15}\,\sin^2(2\,\omega)\right),$$

$$\left(\frac{\Delta t}{\Delta x}\right)^2 \le \frac{257}{480}, \qquad \Delta t \le \frac{\sqrt{7710}}{120}\,\Delta x \le \Delta x. \tag{32}$$

Nonlinear stability theorems are direct by-products of the discrete conservation properties. Method 1 exactly conserves the discrete energy E^n, however

it is not positive definite (the product $(U_{m+1}^{n+1} - U_m^{n+1})\,(U_{m+1}^n - U_m^n)$ is not necessarily greater than zero). Hence no strong nonlinear stability theorem can be proved [17]. However, under the CFL condition, $\Delta t \leq \Delta x$, the discrete energy is positive definite and Method 1 is nonlinearly stable, as proved by Comech and Komech [57]. The nonlinear stability of Methods 2–5 has not yet been studied in the literature.

The nonlinear stability and consistency of Method 1 ensures its convergence thanks to the Lax equivalence theorem. However, in long-time integrations of solutions growing in amplitude, like the kink-antikink collisions under periodic boundary conditions, nonconvergent results have been observed [58, 40]; such problems have not been observed with bounded solutions, like breathers. In the case of Methods 2–5, the linear stability and consistency ensures local convergence thanks to the Lax equivalence theorem. The behaviour of these methods in long-time integrations should be explored.

3. Numerical results

Let us summarize the results obtained for the behaviour in space of Methods 1-5 after an extensive set of simulations for both kink–antikink and breather solution for the sGE. The five methods are compared in terms of global error, energy conservation, computational cost, and behaviour in long-time integrations. Subsection 3.1 presents the results for a kink–antikink collision solution, and Subsection 3.2 for the breather solution.

3.1. Kink–antikink

Let us consider the analytical solution of the sGE given by

$$u_{ka}(x,t) = 4\tan^{-1}\frac{\sinh(v\,(t-10)/r_-)}{v\,\cosh(x/r_-)}, \tag{33}$$

where $r_- = \sqrt{1-v^2}$, and $v = 1/2$, corresponding to a kink–antikink collision. For the validation and comparison of Methods 1–5, the initial conditions (2) are approximated by means of $U_m^0 = u_{ka}(x_m, 0)$, and $U_m^{-1} = u_{ka}(x_m, -\Delta t)$, and the numerical solution U_m^n for $n = 2, 3, \ldots, N$, is calculated for different values of Δt and Δx, always with $T = 20$, $L = 50$, and $\mathrm{Tol} = 10^{-14}$.

Figure 1 (left plot) shows the numerical error $\|U_m^N - u_{ka}(x_m, 20)\|_\infty$ for Methods 1–5 with $\Delta t = 0.001$ as a function of $\Delta x \in [0.001, 1]$. The linear stability conditions in Section 2.1 for $\Delta t = 1/1000$ requires that $\Delta x \geq 1/1000$, $\gtrsim 1/866$, $\gtrsim 1/816$, $\gtrsim 1/764$, and $\gtrsim 1/731$, for Methods 1–5, resp.; hence, in Fig. 1 the plots only show the results when $\Delta x \geq 1/800$, $\geq 1/800$, $\geq 1/700$, and $\geq 1/700$ for Methods 2–5, respectively. The spatial order of the methods can be validated by means of linear fitting of the logarithm of the error versus the logarithm of the grid size when the error in time is smaller than the error in space; in our case, for $\Delta x \in \{0.2, 0.3, \ldots, 1.0\}$, the resulting slopes are given by 2.8, 4.7, 5.0, 7.2, and 8.7, for Methods 1–5, respectively, in agreement with the theoretical consistency order, cf. 2, 4, 4, 6, and 8, resp. Hence, for $\Delta x > 0.1$ the

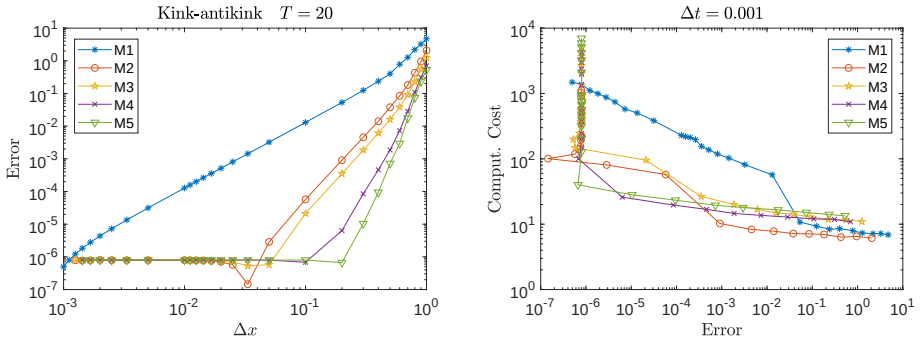

Figure 1: Numerical error (left plot) and computational cost (right plot) for the kink-antikink solution with $T = 20$ and $\Delta t = 1/1000$ as a function of $\Delta x \in \{1/1000,\ 1/900,\ 1/800,\ \ldots,\ 1/100,\ 1/90,\ 1/80,\ \ldots,\ 1/10,\ 2/10,\ 3/10,\ \ldots,\ 1\}$, for Methods 1–5.

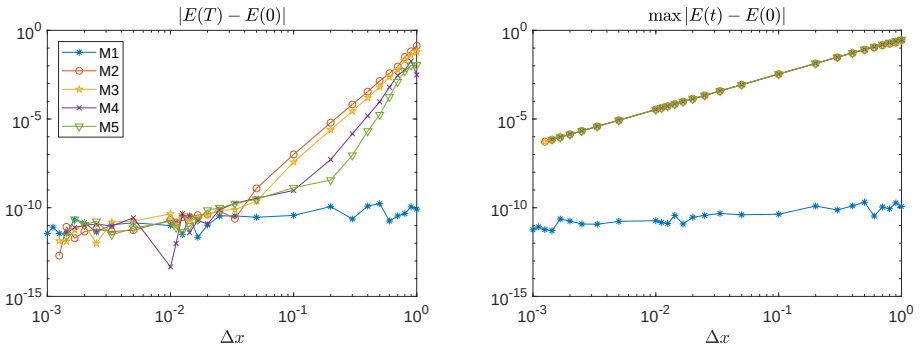

Figure 2: Numerical error of the discrete analogue of the energy (16) for the kink-antikink solution with $T = 20$ and $\Delta t = 0.001$ as a function of $\Delta x \in \{1/1000,\ 1/900,\ 1/800,\ \ldots,\ 1/100,\ 1/90,\ 1/80,\ \ldots,\ 1/10,\ 2/10,\ 3/10,\ \ldots,\ 1\}$, for Methods 1–5. The left plot shows $|E^N - E^0|$, the numerical approximation of $|E(T) - E(0)|$, and right plot shows $\|E^n - E^0\|_\infty$.

high-order methods are more accurate than the lower order ones. However, for $\Delta x \lesssim 0.03$ for Method 2, $\Delta x \lesssim 0.05$ for Method 3, and $\Delta x \lesssim 0.1$ for Methods 4 and 5, the error for Methods 2–5 reaches a constant value $\approx 8.0 \times 10^{-7}$, due to the error in time; such a plateau error can be reduced by using values of $\Delta t < 0.001$.

Figure 1 (right plot) shows the computational cost, estimated by using the run-time in seconds, for Methods 1–5 with $\Delta t = 0.001$ as a function of the numerical error. Method 2 is the most efficient one for errors larger than 10^{-3}, but its cost is similar in magnitude to that of high-order methods. For errors smaller than 10^{-3}, Methods 4 and 5 are the most cost-effective ones, being about tens of times more efficient than Method 1.

The energy of Methods 1–5 is illustrated in Figure 2, where the discrete analogue of the energy (16), exactly conserved by Method 1, has been used instead

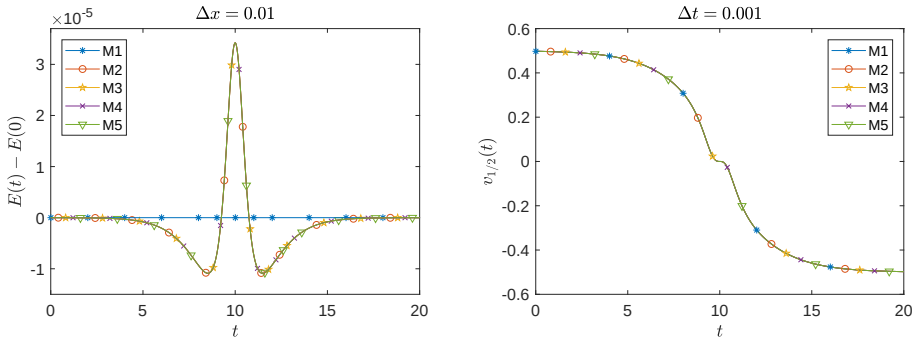

Figure 3: Evolution in time of the energy $E^n - E^0$ (approximation to $E(t) - E(0)$), left plot, and of the speed $V(t)$, right plot, of the kink-antikink solution with $T = 20$, $\Delta t = 0.001$, and $\Delta x = 0.01$, for Methods 1–5.

of a high-order approximation for the exact energy (4); this choice has been motivated by the aim of making a fair comparison of the energy conservation properties among all the methods. Figure 2 shows the value of $|E^N - E^0|$ (left plot) and $\|E^n - E^0\|_\infty$ (right plot) for Methods 1–5 with $T = 20$ and $\Delta t = 0.001$ as a function of $\Delta x \in [0.001, 1]$.

Figure 2 (left plot) shows that, as expected, Method 1 conserves the energy for all Δx, but Methods 2–5 only show good conservation properties for very accurate solutions, when Δx is smaller than ~ 0.04; for larger values of Δx the error in the energy decreases as the grid size does, with a slope that increases with the order of the method.

Figure 2 (right plot) shows that the maximum error in the energy is constant for Method 1, but its value decreases with Δx for Methods 2–5; surprisingly, it coincides among them, being independent of the spatial order of the method. Moreover, this value is $O(\Delta x^2)$, the order of approximation in space of the discrete energy (16). Figure 3 (left plot) shows that the maximum error in the energy is reached at $t = T/2$, where the solution and its spatial derivative becomes null, but its time derivative has a local maximum; in such a point the error in the discrete energy is dominated by the method of integration in time, which is exactly the same for Method 2–5. In our opinion, this is the origin of the features observed in Fig. 2 (right plot).

The speed $v(t) = P(t)/E(t)$ of the exact kink-antikink solution is zero. However, the speed of the kink (antikink) before (after) the collision can be estimated by using the half-interval speed $v_{1/2}(t) = 2\,P_{1/2}(t)/E(t)$, where $P_{1/2}(t)$ is the half-momentum calculated by means of the integration of Eq. (3) in $x \in (-\infty, 0)$; note that, the factor 2 is necessary because the energy is calculated in the whole real line. Figure 3 (right plot) shows the evolution in time of $v_{1/2}(t)$, numerically calculated by the discrete half-momentum, summing for $m \in \{1, 2, \ldots, M/2\}$ in Eq. (17); Methods 1–5 conserve the half-momentum with an error smaller than the resolution of the plot, so the corresponding curves shows overlapped in the

figure. Before the collision, $v_{1/2}(t)$ is the speed of the kink, decreasing monotonically from $v_{1/2}(0) = 1/2$ to $v_{1/2}(T/2) = 0$; during the collision, $v_{1/2}(t)$ shows a tiny plateau, but a careful analysis shows that it is only apparent; after the collision, $v_{1/2}(t)$ is negative, as expected for the speed of the antikink, decreasing monotonically from $v_{1/2}(T/2) = 0$ to $v_{1/2}(T) = -1/2$.

Following Ablowitz et al. [58] and Marsden et al. [40] long-time integration of the kink-antikink solution have been executed for both odd ($M = 255$) and even ($M = 256$) number of spatial nodes, with $v = 1/10$, $L = 40$, $\Delta x = L/M$, $\Delta t = \Delta x/8$, and $T = 200000$, corresponding to an exact solution undergoing 1297 kink-antikink collisions. The results show that the solution of the high-order methods at $t = T$ is not a kink-antikink solution, but it is degraded by the accumulation of round-off errors. Specifically, Method 4 results in unreliable solutions in both even and odd M, but Method 3 only for even M, and Method 5 only for odd M. Ablowitz et al. [58] explained this behaviour depending on the parity of the number of spatial points is due to homoclinic crossings induced by the numerical errors since the initial solution is near a homoclinic orbit. Methods 1 and 2 are stable, but there are errors in the speed of the numerical solitons that result in an incorrect number of collisions with respect to the exact solution. In summary, our best long-time integration results are obtained with Method 2 for both even and odd M, and also with Method 5 but only for even M.

3.2. Breather

The breather solution of the sGE is given by

$$u_{br}(x,t) = 4\,\tan^{-1}\left(\sin(v\,(t-10)/r_+)\,\operatorname{sech}(x/r_+)/v\right), \tag{34}$$

where $r_+ = \sqrt{1+v^2}$, and $v = 1/2$. Let us compare Methods 1–5 with the initial conditions (2) approximated by means of $U_m^0 = u_{br}(x_m, 0)$, and $U_m^{-1} = u_{br}(x_m, -\Delta t)$, and the numerical solution U_m^n for $n = 2, 3, \ldots, N$, is calculated for different values of Δt and Δx, always with $T = 20$, $L = 50$, and $\mathrm{Tol} = 10^{-14}$.

Figure 4 (left plot) shows the numerical error $\|U_m^N - u_{br}(x_m, 20)\|_\infty$ for Methods 1–5 with $\Delta t = 0.001$ as a function of $\Delta x \geq \Delta t$. The estimation of the spatial order of the methods by means of linear fitting for $\Delta x \in \{0.3, 0.4, \ldots, 1.0\}$, results in 2.0, 4.3, 4.8, 6.8, and 8.7, for Methods 1–5, respectively, similar to the expected values of the theoretical consistency order. Hence, for $\Delta x > 0.2$ the high-order methods are more accurate than the lower order ones. However, for $\Delta x \lesssim 0.03$ for Method 2, $\Delta x \lesssim 0.05$ for Method 3, $\Delta x \lesssim 0.1$ for Method 4, and $\Delta x \lesssim 0.2$ for Method 5, the error for Methods 2–5 is dominated by error in time, reaching a constant value $\approx 7.0 \times 10^{-7}$; as expected, using values of $\Delta t < 0.001$, the plateau error can be reduced.

Figure 4 (right plot) shows the run-time (in seconds) for Methods 1–5 with $\Delta t = 0.001$ as a function of the numerical error. Method 2 is the most efficient one for errors larger than 10^{-4}, but its cost is similar in magnitude to that of high-order methods; for errors smaller than 10^{-4}, Method 4 is the most cost-effective one, but Methods 2, and 5 have similar cost.

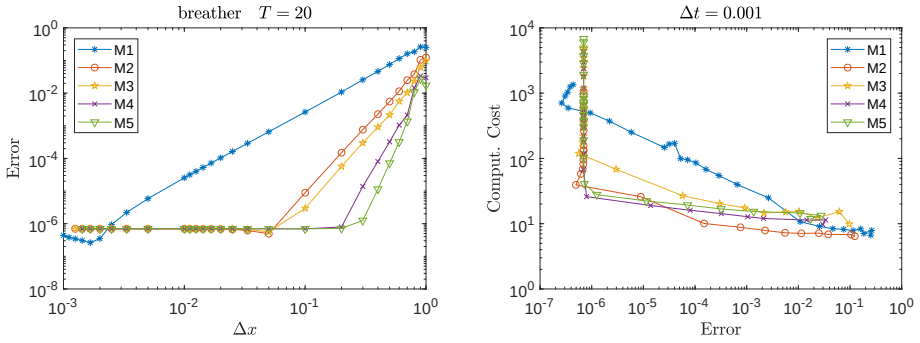

Figure 4: Numerical error (left plot) and computational cost (right plot) for the breather solution with $T = 20$ and $\Delta t = 1/1000$ as a function of $\Delta x \in \{1/1000, 1/900, 1/800, \ldots, 1/100, 1/90, 1/80, \ldots, 1/10, 2/10, 3/10, \ldots, 1\}$, for Methods 1–5.

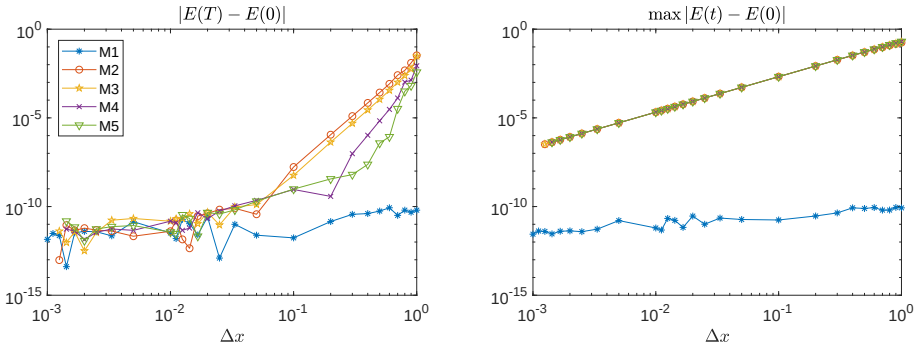

Figure 5: Numerical error of the discrete analogue of the energy (16) for the breather solution with $T = 20$ and $\Delta t = 0.001$ as a function of $\Delta x \in \{1/1000, 1/900, 1/800, \ldots, 1/100, 1/90, 1/80, \ldots, 1/10, 2/10, 3/10, \ldots, 1\}$, for Methods 1–5. The left plot shows $|E^N - E^0|$, the numerical approximation of $|E(T) - E(0)|$, and right plot shows $\|E^n - E^0\|_\infty$.

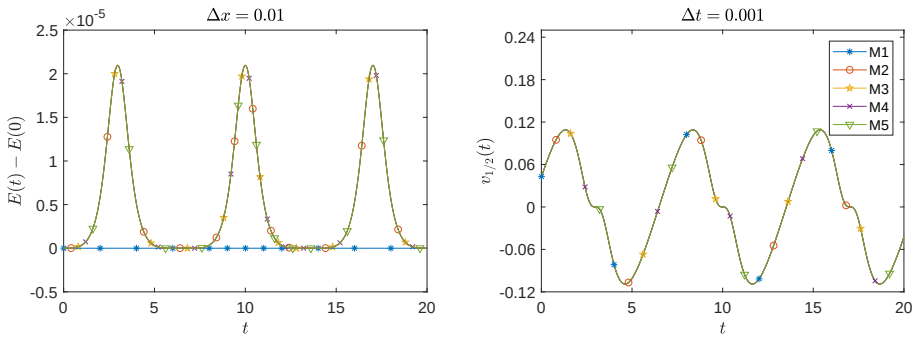

Figure 6: Numerical energy (left plot) and speed (right plot) of the breather solution with $T = 20$, $\Delta t = 0.001$, and $\Delta x = 0.01$, for Methods 1–5.

Figure 5 (left plot) shows that, as expected, Method 1 conserves the energy for all Δx, but Methods 2–5 only show good conservation properties for very accurate solutions, when Δx is smaller than ~ 0.05; for larger values of Δx the error in the energy decreases as the grid size does, with a slope that increases with the order of the method. Figure 5 (right plot) shows that the maximum error in the energy is constant for Method 1, but its value decreases with Δx for Methods 2–5, as previously observed for the kink-antikink solution in Section 3.1. The maximum error in the energy is of the order of approximation in space of the discrete energy (16), i.e., $O\left(\Delta x^2\right)$.

Figure 6 (left plot) shows that the maximum error in the energy for Methods 1–5. It is constant for Method 1, but it oscillates at the same frequency that the breather solution does, for Methods 2–5, with three maxima at $t = 2.98$, 10.0, and 17.0. At these maxima, the breather solution and its spatial derivative becomes null, hence the maximum error in the discrete energy is dominated by the method of integration in time, which is exactly the same for Method 2–5.

Figure 6 (right plot) shows the evolution in time of $v_{1/2}(t)$, cf. Section 3.1, for the numerical breather solution; note that the exact breather has a speed $v(t) = 0$. Methods 1–5 show the same oscillatory behaviour for $v_{1/2}(t)$, thanks to their good conservation properties for the momentum. The value of $v_{1/2}(t)$ oscillates at the same frequency that the breather, with local maxima at $t = 1.33$, 8.36, and 15.4, and local minima at $t = 4.62$, 11.6, and 18.7. Between the maxima and minima there is a tiny plateau, at the same position of the maxima in Fig. 6 (left plot); its origin is similar to the one observed in the kink-antikink solution in Section 3.1.

4. Conclusions

Five numerical schemes for the sGE have been developed and analyzed. All use the same second-order differences in time and the same approximation to the nonlinearity, with a proper rearrangement to avoid catastrophic cancellations in

its numerical evaluation; they are implicit, so Newton's iterative method has been used. Method 1 is the classical Strauss–Vázquez method, interpreted as a (0,2)-Padé numerical method; this method conserves a discrete analog of the energy of the sGE and it is of second-order in space. Methods 2–5 are (0,4)-, (2,2)-, (2,4)-, and (4,4)-Padé methods which fourth-, fourth-, sixth-, and eighth-order of accuracy in space. The local truncation error terms of the five methods have been calculated by using Taylor series expansion. The linear stability of Methods 1–5 has been studied by using the von Neumann analysis, showing that $(\Delta t/\Delta x)^2 \leq 1$, 3/4, 2/3, 7/12, and 257/480, for Methods 1–5, resp.

Methods 1–5 have been compared for both the kink–antikink and breather solutions of the sGE with $\Delta t = 0.001$ and $\Delta x \in [1/1000, 1]$. The results are similar in both cases. For large enough Δx with respect to Δt, the spatial order of the methods has been validated; however, for small Δx the global error is dominated by the contribution of the common method of integration in time. The computational cost (the run-time in seconds) for Methods 1–5 shows that Method 2 is the most efficient one for errors larger than 10^{-3} and 10^{-4} for the kink–antikink and breather solutions, resp.; but for smaller errors Method 4 and 5 are the most cost-effective ones.

Method 1 exactly conserves a discrete energy analogous to the energy of the sGE, but Methods 2–5 shows good conservation properties for accurate solutions, with the error in the energy decreasing as the grid size does, with a slope that increases with the order of the method. In fact, the maximum error in the energy is constant for Method 1, but it is $O(\Delta x^2)$, the order of approximation in space of the discrete energy, for Method 2–5; for the kink-antikink solution this maximum is located at the center of the collision, but for the breather solution oscillates at the same frequency as the breather; in both cases, the maximum is reached where the amplitude and spatial derivative of the solution are null. The speed of the kink (antikink) before (after) the collision in the kink-antikink solution has been estimated using the half-interval speed calculated by the half-interval momentum; the results coincide among Methods 1–5, decreasing monotonically from 1/2 before the collision to $-1/2$ after it, for the kink-antikink solution. The half-interval speed has also been calculated for the breather solution, showing an oscillatory behaviour at the same frequency that the breather.

In long-time integrations, the best results have been obtained by using Method 2, and also Method 5 but only for an even number of spatial points. Method 1 exactly conserves an analogue of the energy, but this property it is not enough to avoid the accumulation of error in the speed of the solitons, that degrades the solution with large amounts of noise (contradicting the theoretical results of convergence published in the literature). For an initial solution near a homoclinic orbit, Method 4 yields noisy solutions for both even and odd number of spatial nodes, Method 3 only for even M, and Method 5 only for odd M.

In summary, our analysis indicates that Method 2 and Method 4 are the most cost-effective ones for small and large error, resp., in short-time integrations, and Method 2 and Method 5, the last one with an even number of spatial points, are the best ones for long-time integrations. Comparing the fourth-order methods,

Method 2 is better than Method 3, even if its local truncation error term is smallest (the sixth-order spatial derivative is multiplied by a smaller number). Comparing the higher-order methods, Method 5 is better than Method 4 for long-time integrations. Except in terms of linear stability, it turns out that the widely used Method 1 is the worst among the other methods studied in this paper, in spite of his energy conservation property.

Our results indicate that to attain a very small global error our high-order methods in space require a high-order scheme in time. There are several possibilities to be explored in the future, either Richardson extrapolation, or diagonally implicit Runge–Kutta–Nyström methods, or even modified equation techniques. The theoretical analysis of the nonlinear stability and convergence of the four novel methods developed in this paper is also an open problem requiring further research.

Acknowledgements

We would like to thank the reviewer for their comments and suggestions for improvement in the overall presentation and clarity of the manuscript. The research reported here was partially supported by Projects EphemeCH (TIN2014-56494-C4-1-P) and DeepBIO (TIN2017-85727-C4-1-P) of the Programa Estatal de Fomento de la Investigación Científica y Técnica de Excelencia del Ministerio de Ciencia e Innovación of Spain.

References

[1] A. Barone, F. Esposito, C. J. Magee, A. C. Scott, Theory and applications of the sine-Gordon equation, Riv. Nuovo Cimento 1 (1971) 227–67.

[2] A. C. Scott, F. Y. F. Chu, D. W. McLaughlin, The soliton: A new concept in applied science, Proc. IEEE 61 (1973) 1443–83.

[3] J. Cuevas-Maraver, P. G. Kevrekidis, F. Williams, The sine-Gordon model and its applications, Nonlinear Systems and Complexity vol. 10, Springer, Berlin, 2014.

[4] M. J. Ablowitz, D. J. Kaup, A. C. Newell, H. Segur, Method for solving the Sine-Gordon equation, Phys. Rev. Lett. 30 (1973) 1262–4.

[5] G. L. Lamb Jr., Elements of soliton theory, Pure & Applied Mathematics, John Wiley & Sons, New York, 1980.

[6] M. J. Ablowitz, H. Segur, Solitons and the inverse scattering transform, SIAM studies in applied mathematics, vol. 4, Society for Industrial and Applied Mathematics, Philadelphia, 1981.

[7] M. J. Ablowitz, P. A. Clarkson, Solitons, nonlinear evolution equations and inverse scattering, London Mathematical Society Lecture Note Series vol. 149, Cambridge University Press, Cambridge, 1991.

[8] F. Martin-Vergara, F. Rus, F. R. Villatoro, Solitary waves on graphene superlattices, in: J. F. R. Archilla, F. Palmero, M. C. Lemos, B. Sánchez-Rey, J. Casado-Pascual (Eds.), Nonlinear Systems, Vol. 2. Nonlinear Phenomena in Biology, Optics and Condensed Matter, Springer, Berlin, 2018, pp. 85–110.

[9] J. K. Perring, T. H. R. Skyrme, A Model unified field equation, Nucl. Phys. 31 (1962) 550–5.

[10] M. J. Ablowitz, M. D. Kruskal, J. F. Ladik, Solitary wave collisions, SIAM J. Appl. Math. 36 (1979) 428–43.

[11] W. Strauss, L. Vázquez, Numerical solution of a nonlinear Klein-Gordon equation, J. Comput. Phys. 28 (1978) 271–8.

[12] P. J. Pascual, L. Vázquez, Sine-Gordon solitons underweak stochastic perturbations, Physical Review B 32 (1985).

[13] S. Jiménez, L. Vázquez, Analysis of four numerical schemes for a nonlinear Klein-Gordon equation, Appl. Math. Computat. 35 (1990) 61–94.

[14] G. Ben-Yu, P. J. Pascual, M. J. Rodriguez, L. Vázquez, Numerical solution of the sine-gordon equation, Appl. Math. Comput. 18 (1986) 1–14.

[15] Z. Fei, L. Vázquez, Two energy conserving numerical schemes for the sine-Gordon equation, App. Math. Comput. 45 (1991) 17–30.

[16] L. Vu-Quoc, S. Li, Invariant-conserving finite difference algorithms for the nonlinear Klein-Gordon equation, Comput. Meth. Appl. Mech. Eng. 107 (1993) 341–91.

[17] L. Vu-Quoc, S. Li, Finite difference calculus invariant structure of a class of algorithms for the nonlinear Klein-Gordon equation, SIAM J. Numer. Anal. 32 (1995) 1839–75.

[18] C. Jiang, W. Cai, Y. Wang, A linear-implicit and local energy-preserving scheme for the sine-Gordon equation based on the invariant energy quadratization approach, arXiv e-prints (2018) arXiv:1808.06854.

[19] M. A. M. Lynch, Large amplitude instability in finite difference approximations to the Klein-Gordon equation, Appl. Numer. Math. 31 (1999) 173–82.

[20] S. Jiménez, Derivation of the discrete conservation laws for a family of finite difference schemes, Appl. Math. Comput. 64 (1994) 13–45.

[21] D. Furihata, Finite-difference schemes for nonlinear wave equation that inherit energy conservation property, J. Comput. Appl. Math. 134 (2001) 37–57.

[22] A. G. Bratsos, E. H. Twizell, The solution of the sine-Gordon equation using the method of lines, Int. J. Comput. Math. 61 (1996) 271–92.

[23] D. Duncan, Sympletic finite difference approximations of the nonlinear Klein-Gordon equation, SIAM J. Numer. Anal. 34 (1997) 1742–60.

[24] A. G. Bratsos, A fourth order numerical scheme for the one-dimensional sine-Gordon equation, Int. J. Comput. Math. 85 (2008) 1083–95.

[25] M. Sari, G. Gürarslan, A sixth-order compact finite difference method for the one-dimensional sine-Gordon equation, Int. J. Numer. Meth. Biomed. Eng. 27 (2011) 1126–38.

[26] A. G. Bratsos, A third order numerical scheme for the two-dimensional sine-Gordon equation, Math. Comput. Simul. 76 (2007) 271–82.

[27] A. G. Bratsos, The solution of the two-dimensional sine-Gordon equation using the method of lines, J. Comput. Appl. Math. 206 (2007) 251–77.

[28] Y. Luo, X. Li, C. Guo, Fourth-order compact and energy conservative scheme for solving nonlinear Klein-Gordon equation, Numer. Meth. Part Differ. Equ. 33 (2016) 1283–304.

[29] C. Wingate, Numerical search for a ϕ^4 breather mode, SIAM J. Appl. Math. 43 (1983) 120–40.

[30] M. J. Ablowitz, B. M. Herbst, C. M. Schober, Numerical simulation of quasi-periodic solutions of the sine-Gordon equation, Physica D 87 (1995) 37–47.

[31] M. J. Ablowitz, B. M. Herbst, C. M. Schober, On the numerical solution of the sine-Gordon equation, J. Comput. Phys. 131 (1997) 354–67.

[32] E. Celledoni, V. Grimm, R. I. McLachlan, D. I. McLaren, D. O'Neale, B. Owren, G. R. W. Quispel, Preserving energy resp. dissipation in numerical PDEs using the "Average Vector Field" method, J. Comput. Phys. 231 (2012) 6770–89.

[33] A. D. Jagtap, A. S. V. Murthy, Higher order scheme for two-dimensional inhomogeneous sine-Gordon equation with impulsive forcing, Commun. Nonlinear Sci. Numer. Simul. 64 (2018) 178–97.

[34] G. W. Wei, D. S. Zhang, D. J. Kouri, D. K. Hoffman, Lagrange distributed approximating functionals, Phys. Rev. Lett. 79 (1997) 775–9.

[35] G. W. Wei, Discrete singular convolution for the sine-Gordon equation, Physica D 137 (2000) 247–59.

[36] B. N. Saray, M. Lakestani, C. Cattani, Evaluation of mixed Crank-Nicolson scheme and Tau method for the solution of Klein-Gordon equation, App. Math. Comput. 331 (2018) 169–81.

[37] J. Argyris, M. Haase, An engineer's guide to soliton phenomena: Application of the finite element method, Comput. Meth. Appl. Mech. Eng. 61 (1987) 71–122.

[38] Y. Shan, W. Liu, B. Wu, Space-time Legendre-Gauss-Lobatto collocation method for two-dimensional generalized sine-Gordon equation, Appl. Numer. Math. 122 (2017) 92–107.

[39] H. S. Shukla, M. Tamsir, V. K. Srivastava, Numerical simulation of two dimensional sine-Gordon solitons using modified cubic B-spline differential quadrature method, AIP Adv. 5 (2015) 017121.

[40] J. E. Marsden, G. W. Patrick, S. Shkoller, Multisymplectic geometry, variational integrators, and nonlinear PDEs, Commun. Math. Phys. 1999 (1998) 351–95.

[41] S. Reich, Multi-symplectic Runge-Kutta collocation methods for Hamiltonian wave equations, J. Comput. Phys. 157 (2000) 473–99.

[42] C. Jiang, J. Sun, H. Li, Y. Wang, A fourth-order AVF method for the numerical integration of sine-Gordon equation, App. Math. Comput. 313 (2017) 144–58.

[43] L. Brugnano, G. F. Caccia, F. Iavernaro, Energy conservation issues in the numerical solution of the semilinear wave equation, App. Math. Comput. 270 (2015) 842–70.

[44] M. Li-Min, W. Zong-Min, A numerical method for one-dimensional nonlinear sine-Gordon equation using multiquadric quasi-interpolation, Chin. Phys. B 18 (2009) 3099–103.

[45] Z.-W. Jiang, R.-H. Wang, Numerical solution of one-dimensional Sine-Gordon equation using high accuracy multiquadric quasi-interpolation, App. Math. Comput. 218 (2012) 7711–6.

[46] M. Dehghan, A. Shokri, A numerical method for solution of the two-dimensional sine-Gordon equation using the radial basis functions, Math. Comput. Simul. 79 (2008) 700–15.

[47] A. Hussain, S. Haq, M. Uddin, Numerical solution of Klein-Gordon and sine-Gordon equations by meshless method of lines, Eng. Anal. Bound. Elem. 37 (2013) 1351–66.

[48] X. Xu, Z. Lu, X. Luo, A numerical meshless method of soliton-like structures model via an optimal sampling density based kernel interpolation, Comp. Phys. Commun. 192 (2015) 12–22.

[49] J. I. Ramos, The sine-Gordon equation in the finite line, App. Math. Comput. 124 (2001) 45–93.

[50] M. Dehghan, D. Mirzaei, The dual reciprocity boundary element method (DRBEM) for two-dimensional sine-Gordon equation, Comput. Meth. Appl. Mech. Eng. 197 (2008) 476–86.

[51] M. Baccouch, Optimal energy-conserving local discontinuous Galerkin method for the one-dimensional sine-Gordon equation, Int. J. Comput. Math. 94 (2017) 316–44.

[52] M. Baccouch, Superconvergence of the local discontinuous Galerkin method for the sine-Gordon equation in one space dimension, J. Comput. Appl. Math. 333 (2018) 292–313.

[53] R. Flesch, M. G. Forest, A. Sinha, Numerical inverse spectral transform for the periodic sine-Gordon equation: Theta function solutions and their linearized stability, Physica D 48 (1991) 169–231.

[54] B. Deconinck, T. Trogdon, X. Yang, Numerical inverse scattering for the sine-Gordon equation, arXiv e-prints (2018) arXiv:1806.10709.

[55] L. T. K. Nguyen, A numerical scheme and some theoretical aspects for the cylindrically and spherically symmetric sine-gordon equations, Commun. Nonlinear Sci. Numer. Simul. 36 (2016) 402–18.

[56] R. Buckingham, P. D. Miller, Exact solutions of semiclassical non-characteristic cauchy problems for the sine-gordon equation, Physica D 237 (2008) 2296–341.

[57] A. Comech, A. Komech, Well-posedness and the energy and charge conservation for nonlinear wave equations in discrete space-time, Russ. J. Math. Phys. 18 (2011) 410–9.

[58] M. J. Ablowitz, B. M. Herbst, C. M. Schober, On the numerical solution of the sine-Gordon equation: I. Integrable discretizations and homoclinic manifolds, J. Comput. Phys. 126 (1996) 299–314.